Microporous and Mesoporous Materials 350 (2023) 112318

Contents lists available at ScienceDirect

Microporous and Mesoporous Materials

journal homepage: www.elsevier.com/locate/micromeso

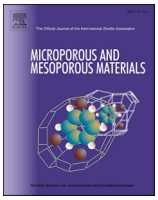

# Functionalized modulators in imine-linked covalent organic frameworks (COFs)

Ellen Dautzenberg, Frank W. Claassen, Louis C.P.M. de Smet *

*Laboratory of Organic Chemistry, Wageningen University, Stippeneng 4, 6708 WE, Wageningen, the Netherlands*

ARTICLE INFO

*Keywords:*
Covalent organic frameworks
Porous materials
Schiff chemistry
Dynamic covalent chemistry
Modulators
Gas separation

ABSTRACT

Covalent Organic Frameworks (COFs) are porous materials with high surface areas, making them interesting for a large variety of applications including energy storage, chemical sensing, and gas separation. In gas separation and sensing, functionalization beyond the COF linkage can result in selective COF-gas interactions, tailoring the properties for the desired application. However, not all functional groups are compatible with the synthetic conditions needed for COF formation. Modulators, which are typically monovalent building blocks that would terminate the reaction, have been shown to maintain or even improve the COF porosity by slowing down the reaction kinetics. Herein, we report on a series of several *para*-functionalized (OMe, Me, F, Cl, $CF_3$, $NO_2$) amine modulators to introduce additional functionality into the framework to study the selective $CO_2/N_2$ gas separation under flue gas conditions. Thorough characterization of the modulated COFs showed that the modulators are located on the outside of the polymeric sheet and get replaced by benzidine molecules, favoring a regular network formation over a homogeneous modulator distribution. The fractions of eventually incorporated modulator vary per functional group between 2.1% ($NO_2$-modulated COF) and 8.9% (Me-modulated COF) while maintaining high BET surface areas (>1800 $m^2/g$). It was found that all modulated COFs adsorb moderate quantities of $CO_2$ and show comparable $CO_2/N_2$ IAST selectivity values under flue gas conditions. A higher number of functional groups in the framework was shown to enhance the IAST selectivity.

## 1. Introduction

Porous materials are solid materials, possessing permanent pores with pore sizes of a few to several hundred nanometers. These pores can be classified into macro- (>50 nm), meso- (2–50 nm) and micropores (<2 nm) [1]. In 2005, Yaghi and co-workers reported the first Covalent Organic Framework (COF) as a new type of fully organic porous nanomaterial [2]. Since then, COFs have gained increasingly more interest and a huge variety of different materials and applications have been reported [3,4]. The permanent porosity and their channel-like structure lead to high surface areas, which are of interest for, amongst others, energy storage [3,5], chemical sensing [3,6], photocatalysis [3,7,8] and gas separation [3,9]. COFs are usually synthesized via polycondensation of two multifunctional building blocks. The formed COF linkages are based on Dynamic Covalent Chemistry (DCC) [10,11]. DCC refers to reversible reactions carried out under thermodynamic reaction conditions, which enable error correction within the reaction. This leads to a crystalline framework with long-range order. Imines are known for DCC, which makes them interesting for COFs. They can be synthesized in a condensation reaction from aldehyde and amine building blocks with an acidic catalyst, which is also known as Schiff base chemistry [3,12–14].

In the context of gas separation applications, COFs are exposed to a mixture of gases of which one gas would – ideally – selectively adsorb onto the COF surface and inside the COF pores. Here, the porosity of COFs is advantageous to store large quantities of gas, which has, for instance, been used for carbon dioxide capture and storage. As the term 'gas separation' already states, it is important to have a selective adsorption of one gas over another, in order to achieve the desired separation. In fact, the development of new, more selective, porous materials for carbon dioxide capture crucially depends on the ability to determine this gas selectivity. Measuring mixed-gas adsorption requires specialized and expensive equipment [15]. The measuring principle relies on dynamic methods, in which the gas mixtures are constantly flowing over the sample and so-called breakthrough curves are recorded to determine how much of which gas is adsorbed. In contrast, measuring the adsorption isotherm of a pure component is far more straightforward and is possible with common physisorption instruments. Physisorption instruments measure the quantity of gas adsorbed at each pressure,

* Corresponding author.
*E-mail address:* louis.desmet@wur.nl (L.C.P.M. de Smet).

https://doi.org/10.1016/j.micromeso.2022.112318
Received 5 August 2022; Received in revised form 19 October 2022; Accepted 24 October 2022
Available online 3 November 2022

leading to isotherms of the pure gases.

In order to determine gas separation selectivity values out of pure component isotherms, the so-called Ideal Adsorption Solution Theory (IAST) was developed by Myers and Prausnitz [16]. The basis of IAST is analogous to Raoult's law [16]. Both theories assume a linear dependence between gas pressure and the mole fraction of the gaseous component; in case of Raoult's law the vapor pressure and in IAST the equilibrium gas-phase pressure [16]. The simplicity of these calculations makes IAST a widely used method for selectivity determination in gas separation. The IAST selectivity $S$ of a binary gas mixture in IAST is defined as the ratio of the mole fractions in the adsorbed state ($q$) over the mole fractions of the bulk phase ($p$) of components 1 and 2 (Equation (1)) [17].

$$S = \frac{q_1 \times p_2}{q_2 \times p_1} \quad (1)$$

The validity of IAST has been studied by comparing the IAST results with grand canonical Monte Carlo (GCMC) simulations for Metal Organic Frameworks (MOFs) [18]. Despite the development of more accurate GCMC simulations over the past decades, the obtained selectivity predictions, as well as experimentally obtained data, are still comparable to IAST predictions [19–25]. The comparable results of IAST with GCMC simulations, its simplicity and general applicability are the reason why IAST is still the benchmark theory for mixed adsorption studes.

Being a primary greenhouse gas, $CO_2$ plays an important role in climate change. Strategies to mitigate global warming include the reduction of $CO_2$ emissions via carbon capture and storage. The separation of $CO_2$ from $N_2$ – and the associated $CO_2/N_2$ selectivity – play a crucial role in such strategies. In this context, the porosity of COFs is advantageous to store large quantities of gas [26,27]. Computational studies have shown that metal doping significantly increases the $CO_2$ uptake at 298 K and 1 bar [28]. Among the screened metals (Li, Na, K, Be, Mg, Ca, Sc, Ti), the $CO_2$-metal interaction is best in terms of adsorption and desorption for Li. The $CO_2$ uptake and $CO_2/N_2$ selectivity have been investigated under high pressure (>1 bar) or flue gas (15% $CO_2$, 1 bar) conditions for example. It was found that the $CO_2$ adsorption increases with increasing pressure. At 5 bar pressure, triazine-based $\beta$-ketoenamine COF reached a $CO_2$ adsorption of 12.97 mmol/g and 3.64 mmol/g at 273 K and 298 K, respectively [29]. Flue gas conditions are relevant for the purification of industrial exhaust gases and several COFs have been investigated under those conditions. Covalent Triazine Frameworks (CTFs), a special type of COFs, are reported to have high $CO_2/N_2$ selectivities. Mahato et al. reported the highest $CO_2/N_2$ IAST selectivity value for COFs under those chosen flue gas conditions so far of 185.8 at 273 K with an $CO_2$ adsorption of 3.50 mmol/g [30]. Among COF materials, imine COFs are most commonly used and Huang et al. synthesized an porphyrin COF, whose channel-walls were post-synthetically functionalized with carboxyl groups [26]. The selectivity under the above mentioned conditions was enhanced by more than ninefold compared to the pristine COF to $S = 77$. Das et al. studied an imine network and determined $CO_2/N_2$ selectivities of 211 at 273 K and 100 at 298 K [31]. These values were validated by breakthrough experiments, leading to a selectivity of 125 at 298 K, which is even higher than predicted by IAST. Structure-performance studies of six different COFs, carried out by Wang et al., have revealed that $\beta$-ketoenamine COFs outperform imine COFs with similar pore sizes [32]. They did not find a direct relation between the $CO_2$ uptake and the pore size.

Research has not been limited to carbon dioxide separation, but also sulfur dioxide ($SO_2$) removal from flue gas by COFs has been studied [33]. Imide-linked COFs were functionalized by incorporation of 4-[(dimethylamino)methyl]aniline and the $SO_2$ uptake was measured over time, leading to 6.30 mmol $SO_2$ $g^{-1}$, which is equivalent to 40 wt%.

Such monovalent amines or aldehydes can be used as modulators. Modulators would terminate the polymerization. Due to the dynamic nature of imine chemistry, the imine bonds can react back to the starting materials again or undergo metathesis and the modulator can be replaced by a diamine to continue polymerization. This dynamic behavior enables two different possibilities how the modulator acts during polymerization: (1) the modulator is homogenously distributed, leaving some pores unclosed and therefore disrupts the regular framework, resulting in a non-ideal honeycomb structure or (2) the modulator is heterogeneously distributed. In several studies, it has been shown that the mostly unfunctionalized modulator was mainly located on the outside of the 2D polymeric sheet, acting as a capping agent [34–37]. Calik et al. studied the position of the modulator by using a thiol-functionalized modulator to enable staining with iridium clusters [38]. High-angle annular dark-field scanning Transmission Electron Microscopy showed that the stained modulators were mainly located at grain boundaries. Moreover, Lee et al. used a dimethylamine-functionalized modulator in imide COFs for $SO_2$ capture [33]. Since the polymerization is dynamic, the modulator gets constantly replaced by diamine molecules. This exchange reaction slows down the framework polymerization and leads to a more regular framework [34,35,37–42]. In general, such modulators can additionally contain different functional groups [33], ranging from electron-withdrawing groups to electron-donating groups. The influence of such functional groups was studied by Hammett et al. who derived an equation that correlates the chemical structure with the corresponding reactivity [43,44]. Later Hansch et al. compiled extensive lists of Hammett parameters for a broad library of functional groups [45,46]. The applicability of the Hammett equations has been shown in several studies, amongst others the hydrolysis of *p*-nitrophenyl benzoate esters [47], imine exchange in multistep metallo-organic transformations [48] or imine exchange in covalent adaptable networks [49].

As shown by these examples, functional groups play an important role in tailoring the selectivity of COFs for gas adsorption and modulators have proven to form COFs with high porosity. Therefore, we decided to extend this approach by employing a series of functionalized modulators, which are even commercially available. The obtained materials were thoroughly characterized and the modulator concentrations within the framework were determined. Additionally, the impact of the different functional groups on $CO_2/N_2$ selectivity under flue gas conditions was systematically studied.

## 2. Experimental

### 2.1. Materials

Benzidine (98%) was purchased form Abcr, *p*-anisidine, *p*-toluidine, 4-fluoroaniline, 4-chloroaniline, 4-trifluoromethylaniline, and 4-nitroaniline were purchased from Sigma Aldrich, and all chemicals were used without further purification. Mesitylene (99%, extra pure) was purchased from Fisher Scientific and 1,4-dioxane (99%) was purchased from Acros Organics B.V.B.A. 2,5,6-Trimethyl-1,3,5-benzenetricarboxaldehyde was synthesized before [50]. All solvents and glacial acetic acid (AR) were purchased from commercial sources and used without further purifications.

### 2.2. Methods

$^1$H spectra were recorded on a Bruker AVANCE III NMR spectrometer at 600 MHz. The spectra were referenced with respect to the deuterated solvents (DMSO-$d_6$: 2.5 ppm). The spectra were analyzed using MestReNova (version 14.1.0).

FT-IR spectra were obtained on a Bruker Tensor 27 spectrometer with an attenuated total reflection accessory called Platinum. The samples were applied as powder on top of the crystal. 64 scans were performed with a resolution of 4 $cm^{-1}$.

Powder X-Ray diffraction measurements were performed with a Philips X'pert-PRO at 40 kV and 40 mA from 4 to 40° (step size: 0.05°,

step time: 90 s, mask in front of entrance: 10 mm and slit 1°, slit before detector: 1°) and from 1.5 to 10° (step size: 0.05°, step time: 500 s, mask in front of entrance: 5 mm and slit 0.5°, slit before detector: 0.25°). X-Rays were generated by a Cu anode K$\alpha$ (1.54 $\lambda$) radiation. The goniometer radius was 240 mm, the soller slits were 2.3° and the receiving slit was 0.1 mm in width. Pawley refinement was carried out in Topas (version 5) with a CuKα5_Berger emission profile. The parameters "Zero point error", "Cry Size L" and "Strain L" were allowed to refine.

X-Ray photoelectron spectroscopy (XPS) measurements were performed using a JPS-9200 photoelectron spectrometer (JEOL, Ltd., Japan). Samples were pressed on indium foil. All samples were analyzed using a focused monochromated Al Kα X-ray source (spot size of 300 μm) at a constant dwelling time for survey scan 50 ms and pass energy = 50 eV. The power of the X-ray source was 240 W (20 mA and 12 kV). Charge compensation was applied during the XPS scans with an accelerating voltage of 2.8 eV and a filament current of 4.8 A. XPS survey-scan spectra were obtained under ultrahigh vacuum conditions (base pressure = $3 \times 10^{-7}$ Pa). The survey scans were integrated with a Shirley background using CasaXPS. All spectra were referenced to the C1s peak attributed to C-C and C-H atoms at 285.0 eV.

Nitrogen adsorption-desorption measurements for surface area determination were performed on a MicroActive for Tristar II Plus 3030 at 77.350 K with an equilibration time of 10 s and a non-ideality factor of $6.2 \times 10^{-5}$. Before the measurement, the samples were outgassed at 120 °C overnight. Surface areas were calculated from the adsorption data using Brunauer-Emmett-Teller (BET) methods and Roquerol criteria. The pore-size distribution curves were obtained from the adsorption branches using HS-2D-NLDFT, Carbon Cylindrical Pores (ZTC), $N_2$@77K. An optimum between Goodness of Fit and smoothness of the pore size distribution was aimed for. The average of three different COF batches was used to determine the BET surface areas.

Nitrogen and carbon dioxide adsorption measurements were performed at 295 K with absolute pressure dosing and an equilibration time of 20 s between 3 and 1200 mbar. The free space values were determined after the adsorption measurement. Nitrogen measurements at 273 K were performed under the same conditions as 295 K. Carbon dioxide measurements at 273 K were performed by increment dosing up to $p/p^0 = 0.03$ with an increment of 0.13384 mmol/g and an equilibration time of 20 s. The gases were considered as ideal gases under all these circumstances.

The $CO_2/N_2$ selectivities were predicted based on the Ideal Adsorption Solution Theory (IAST) [16,51] by GraphIAST [52] at 1 bar and a composition of 0.15/0.85. The isotherms were fitted with the interpolator model. Negative adsorption values in the low pressure range were left out of the IAST calculations.

Thermogravimetric analysis was performed on a PerkinElmer STA 6000. The sample was heated to 30 °C and this temperature was maintained for 1 min, before the sample was heated with 10 °C/min to 700 °C in a nitrogen atmosphere with a flow rate of 20 ml/min. The thermal stability was determined at the point where 95% of the sample were still retained.

Scanning electron microscopy images have been recorded with a Jeol JAMP-9500F. The samples were pretreated with a goldsputter (Jeol JFC-1300) with 40 s sputtering time. The images were recorded at 5.0 kV at different magnifications.

Origin2020b (64-bit) version 9.7.5.184 was used to analyze, to plot and to fit all data.

### 2.3. Synthesis

The COF synthesis is based on a modified procedure of Smith et al. [53]:

The aldehyde (1 equiv.) and the modulator (3 equiv.) were dissolved in 4:1 *v/v* 1,4-dioxane:mesitylene mixture in a 50 mL round bottom flask, together with a stirring rod. The solution was heated for 2–5 min to 70 °C and glacial acetic acid (1.0 mL) was added. The reaction mixture was stirred at 70 °C for 1 day. Benzidine (1.05 equiv.) and glacial acetic acid (0.8 mL) were added and a yellow precipitate was formed. The reaction mixture was stirred at 70 °C for 1 day. Afterwards, the reaction was cooled to RT and the precipitate was collected via Büchner filtration. The solid was dispersed in dimethylformamide (DMF), stirred at 90 °C for 30 min and collected via Büchner filtration. These steps were repeated with DMF (90 °C, 30 min), ethanol (80 °C, 30 min), acetone (60 °C, 30 min) and hexane (70 °C, 30 min). After the final Büchner filtration, the COFs were dried overnight at 120 °C in a regular oven. After drying, the COFs were kept in the glovebox for storage.

OMe-modulated COFs were heated for 2 days after the addition of benzidine.

## 3. Results and discussion

In a first approach to introduce functional groups in our imine-linked COFs [50], we have tried to react several *ortho*-substituted (OMe, OH, F, $NO_2$) benzidine building blocks with our recently reported methyl aldehyde building block [50]. While the methoxy-substituted benzidine resulted in a COF (SI Figs. 1–3), the hydroxy-substitution led to an amorphous network (SI Figs. 4–6), and fluoride- and nitro-substitution did not react at all. The electron-withdrawing character of fluoride- and nitro-substitution leads likely to a decrease in reactivity and thus no reaction could be observed. We therefore looked into a different strategy to incorporate those functional groups in our COFs and decided to continue via *para*-substituted modulators (Scheme 1).

### 3.1. Synthesis, reaction optimization and characterization of COFs with modulators

In a classical *Schiff base* condensation reaction, two equivalents of aldehyde node and three equivalents of amine linker were reacted at 70 °C in 1,4-dioxane:mesitylene 1:4 *v/v* at atmospheric pressure. The three equivalents of amine linker consist together out of benzidine and the respective modulator. With the amount of modulator added, we were aiming for approximately 30 mol% of modulator of all amines in the framework. This will be abbreviated as "mol% modulator". With the chosen building block, more than 30 mol% of modulator would decrease the number of functional groups for imine formation per monomer below two, which would interfere with the formation of a regular framework.

In a one-pot synthesis of $CF_3$-modulated COF, only ~3% modulator was found based on digestion $^1$H NMR. In order to get higher quantities of modulator incorporated into the framework, the reaction conditions were optimized. In a first step, the modulator was reacted quantitatively with all aldehyde groups of $Me_3$TFB, to which then 70 mol% benzidine was added *in situ*, and an immediate precipitation could be observed (Scheme 1). The precipitate was isolated after 6 h, 1 d, 2 d and 3 d and the BET surface area was determined to check the porosity. It was found that the BET surface area after 1 day of reaction time was 2028 $m^2/g$ and did not change much anymore upon further increased reaction times (SI Table 2). Since a trade-off between the concentration of functional groups within the framework and porosity is needed, the COFs were also digested in DCl/$D_2O$ before $^1$H NMR analyses to calculate the fraction of modulator. The concentration of modulator decreases over time, which means that the reactivity of benzidine is higher compared to the reactivity of modulator. This indicates that it is thermodynamically advantageous to form a crystalline framework rather than incorporating all functional monomers into the polymers, as that would lead to interrupted networks.

The synthesis of methoxy-modulated COFs required different reaction conditions, because initially, before optimization, no precipitate and thus no COF was formed. Instead, $Me_3$TFB and 30 mol% OMe-modulator were reacted for one day before benzidine was added and allowing the reaction to proceed for another two days.

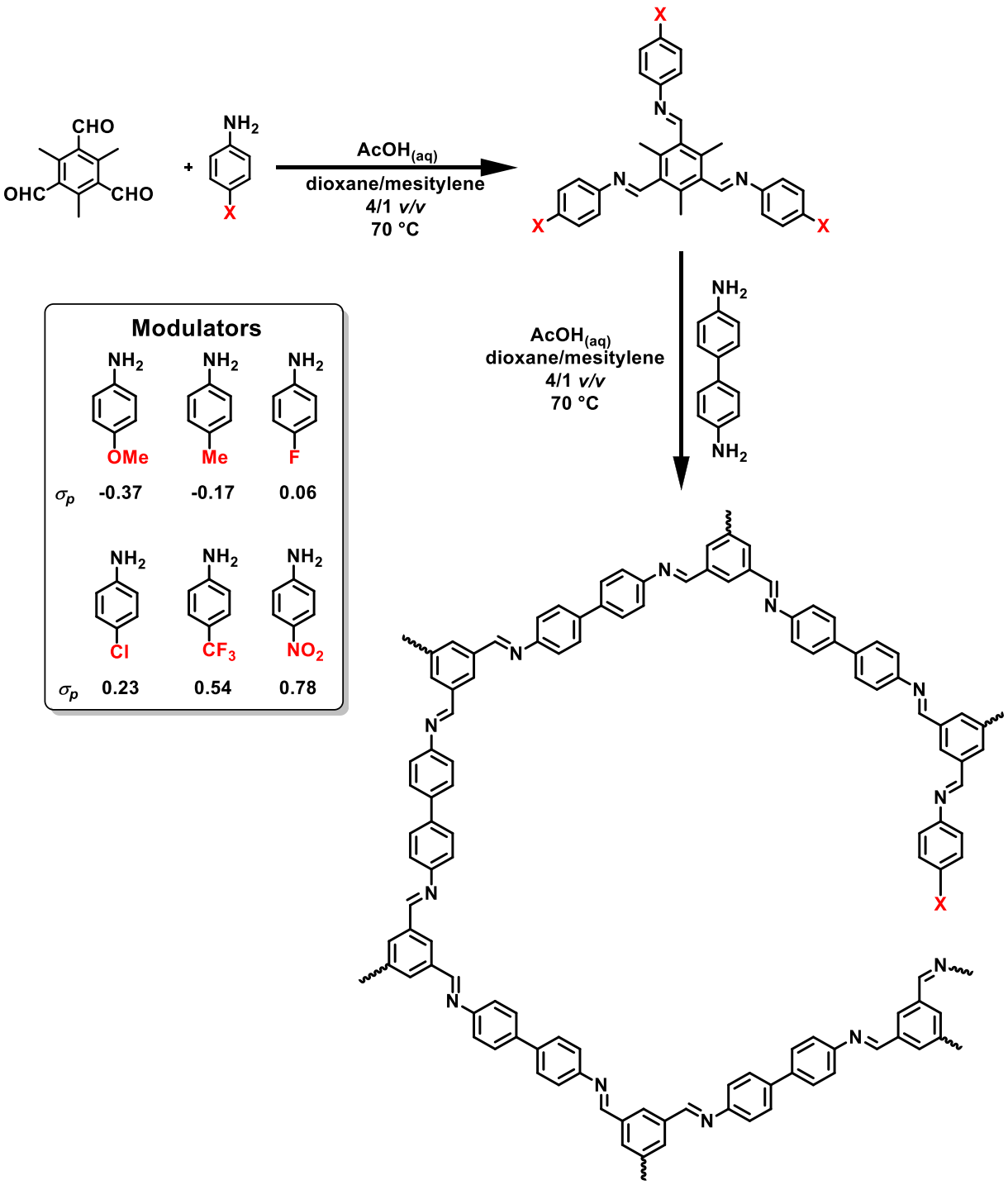


**Scheme 1.** Schematic showing the synthesis of modulated COFs in a two-step reaction. In the inset all *para*-substituted modulators used in this study, including their Hammett parameters, are given.

After this reaction optimization, all modulator-functionalized COFs have been synthesized and characterized in triplicate. The COFs were isolated by Büchner filtration and subjected to Vitaku et al.'s extensive washing procedure [13]. The material was then dried at 120 °C overnight in an air-ventilated oven. The characterization of modulated COFs is exemplarily demonstrated for $CF_3$-modulated COF, because this modulator can easily be recognized by Fourier-Transform Infrared Spectroscopy (FT-IR). The characterization for the other modulated COFs can be found in the Supporting Information.

As a first step, to confirm the successful COF formation, FT-IR was performed, yielding an almost identical spectrum as the spectrum of $Me_3$TFB-BD COF (Fig. 1A). Additionally, characteristic bands of the modulator 4-trifluoromethylaniline can be identified, *i.e.*, the strong bands at 1319, 1099 and 1061 $cm^{-1}$, which are characteristic for $CF_3$ groups [54]. The absence of bands at 1319 $cm^{-1}$ and 1061 $cm^{-1}$ in the FT-IR spectrum of $Me_3$TFB-BD shows that the that modulator has been incorporated. The band at 1099 $cm^{-1}$ overlaps with other COF-related bands and are therefore not clearly visible. The incorporation of the other modulators is less visible in the IR spectra (SI Figs. 7–11).

Powder-X-Ray Diffraction (PXRD) analysis was carried out to study the crystallinity. The diffractogram of $CF_3$-modulated COF – as well as the diffractograms of all other modulated COFs (SI Figs. 12–17)– show

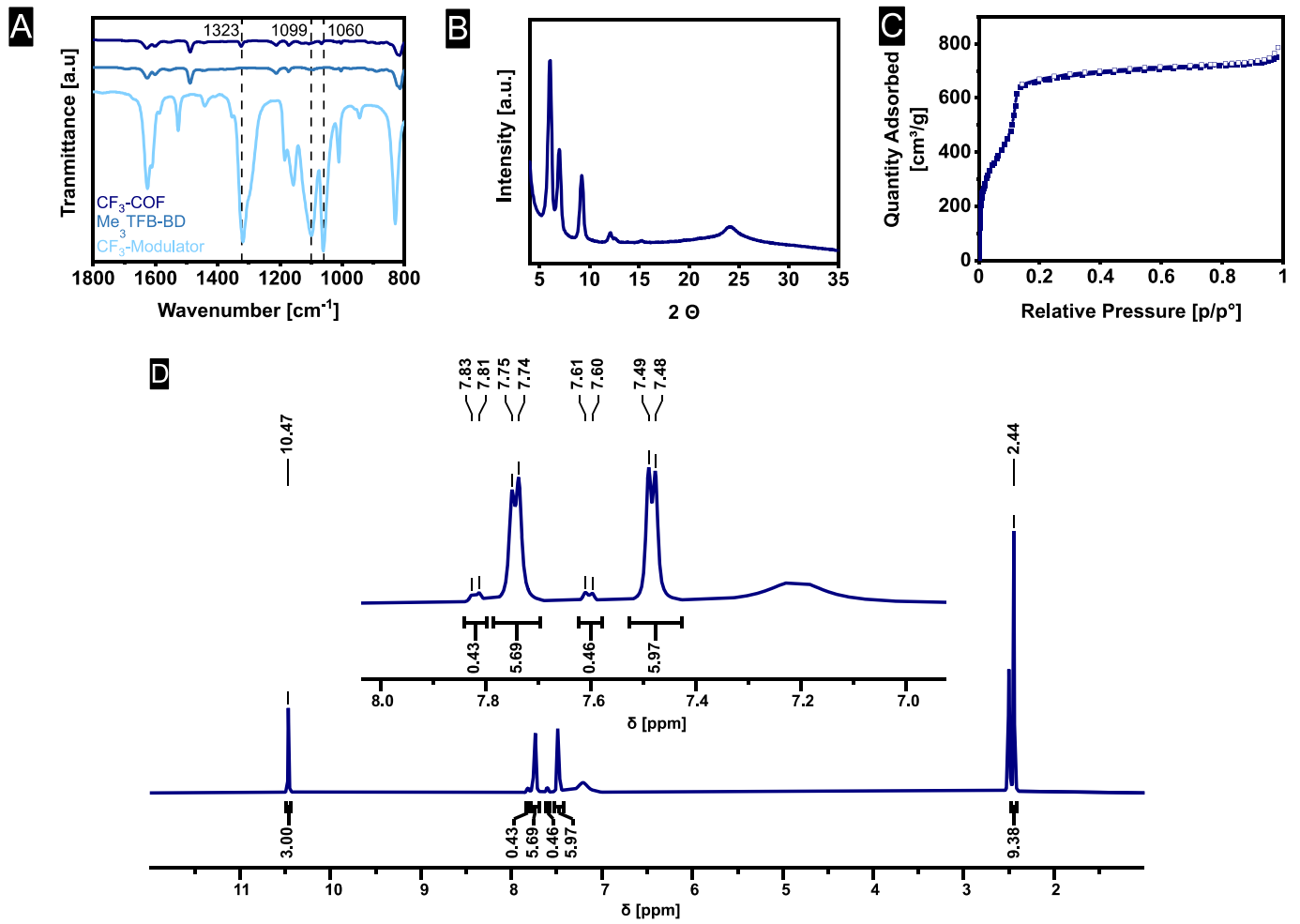


**Fig. 1.** Characterization of the $CF_3$-modulated $Me_3$TFB-BD COF: (A) FT-IR spectrum, (B) PXRD diffractogram, (C) adsorption-desorption isotherm, (D) and NMR digestion to quantify the modulator content. The dashed lines in the FT-IR spectrum indicate the characteristic bands of the modulator 4-trifluoromethylaniline.

the same diffraction peaks as $Me_3$TFB-BD (Fig. 1B), confirming the crystallinity of all COFs. Pawley refinement was performed in triplicate with the PXRD diffractograms using space group *P6/m*, which corresponds to an eclipsed stacking structure. The unit cell dimensions and $R_{wp}$ and $R_p$ values are given in SI Table 1. The unit cell parameters match with those of $Me_3$TFB-BD, confirming the same crystal structure [55].

Nitrogen sorption experiments have been carried out to determine the porosity and BET surface area of all COFs. The type IVb isotherm of $Me_3$TFB-BD with a pore size of 2.7 nm is retained in $CF_3$-modulated COF (Fig. 1C). All other modulated COFs also have a type IVb isotherm with a pore size distribution centered at 2.7 nm (SI Figs. 19–24). A pore size of 2.7 nm is just in between micro- and mesoporosity and the microporosity is shown by a large adsorption of nitrogen in the low pressure range ($p/p^0$<0.1). A step in the isotherms at $p/p^0$=0.1 indicates capillary condensation. The isotherms do not show a hysteresis during desorption. The comparable isotherm shape and pore size distribution of $Me_3$TFB-BD and all modulated COFs is in line with the comparable PXRD diffractograms and the low fractions of modulators in the COFs, pointing to the similarities in the structures of the functionalized, modulated COFs and $Me_3$TFB-BD. The adsorption branches were used to calculate the BET surface area ($S_{BET}$). All samples are microporous, which means the original $p/p^0$ range from 0.05 to 0.3 is not applicable. Therefore, lower relative pressures have been used for the linear fit and the Rouquerol criteria [56] were applied. The same pressure range has been used for the linear fit of the same COF. A BET surface area of 1966 ± 54 $m^2/g$ was found for $CF_3$-modulated COF.

Since the IR spectra could not unambiguously show the presence of the modulator inside the COF, it was proven and quantified by NMR digestion. In NMR digestion, the COF sample is cleaved into its monomers again for the purpose of COF analysis (SI Figs. 25–29). In more detail, the sample was exposed to DCl in $D_2O$ solution in deuterated DMSO-$d_6$, and the $^1$H NMR spectrum was measured (Fig. 1D). The resulting spectrum shows a signal at 10.47 ppm, which is a characteristic chemical shift for aldehyde protons, indicating that the COF is depolymerized. The four doublets between 7 and 8 ppm correspond to the arylic protons of the benzidine and the modulator. After phase and baseline correction, the signals were integrated and based on the integrals, the amount of modulator in mol% was calculated. For $CF_3$-modulated COFs, 7.4 ± 0.4 mol% modulator is incorporated within the framework, which is significantly less than the 30 mol% feed. This shows that the polymerization with benzidine is favorable compared to maintaining the modulator-aldehyde imine bonds. Since there is not enough benzidine to react with all aldehyde groups, the yield of COF precipitate would also reduce, which was confirmed by our experiments.

Comparing the entire range of modulated COFs, the BET surface areas are between 1857 ± 247 $m^2/g$ and 2097 ± 141 $m^2/g$ and do not vary much depending on the modulator used (Fig. 2). Such high BET surface areas translate to a high number of adsorption sides for gases, which makes these materials promising for gas applications. The amount of modulator that has been incorporated into the framework is repeatable for a specific modulator, which can be seen by the small error margins. The amount of modulator varies significantly depending on the modulator used and ranges from 2.1 ± 0.2 mol% for $NO_2$-modulated COFs to 8.9 ± 0.1 mol% for Me-modulated COFs (Fig. 2, SI Table 3).

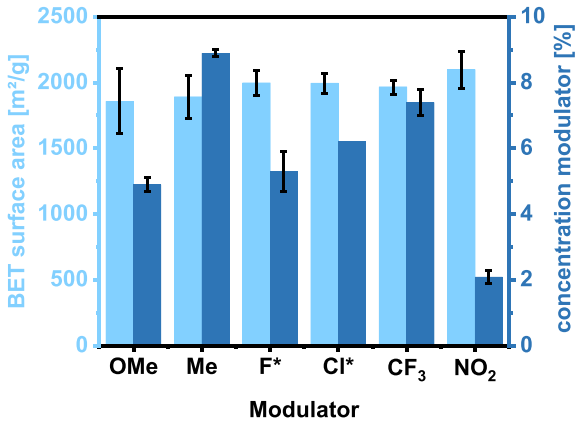


**Fig. 2.** Average BET surface areas (left axis) of all modulated COFs and the concentration of modulator incorporated into the framework in mol% of amines (right axis). The errors bars result from the analyses of triplicates, apart from the modulator concentration of F-modulated COF, which were performed in duplicate (SI section $^1$H NMR Digestion).

There is no trend from the Hammett parameter to the amount of modulator within the COF, which allows to synthesize COFs with varying functional groups to get comparable materials in terms of their BET surface area, crystallinity, and degree of functionalization.

To investigate the spatial arrangement of the modulator, X-Ray Photoelectron Spectroscopy (XPS) wide scans have been measured for the F-modulated COF in triplicate at two different spots for each sample (Fig. 3). XPS is a technique to analyze the surface of a sample and it has a high sensitivity for fluorine [57,58]. Based on the F1s signal intensity, the fraction of modulator at the surface of the COF sample is estimated to be 22 ± 8 mol% (Table 1). As this value is much higher compared to the 5.3 ± 0.6 mol% determined by $^1$H NMR digestion of the bulk powder, the modulator is mostly located at the surface.

The diffraction pattern indicates a regular framework formation, which means that a $Me_3$TFB-BD framework is formed in the bulk, containing modulator units on the outside of the 2D polymeric sheets. This finding is in line with recent literature [34–38].

The thermal stability was studied by thermogravimetric analysis (TGA) (SI Fig. 30). $Me_3$TFB-OMeBD started to decompose at 366 °C and all modulated COFs started to decompose between 410 and 418 °C (SI Table 4). The type of functional group of the modulator therefore have no effect on the thermal stability of the COF. All thermal stabilities are comparable to the one of $Me_3$TFB-BD [50].

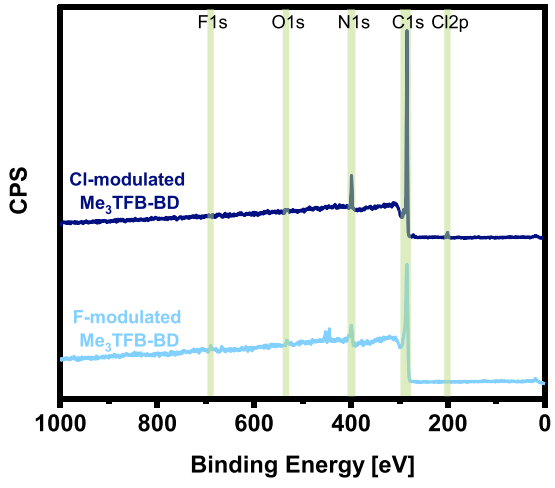


**Fig. 3.** XPS survey scan of Cl-modulated and F-modulated COFs.

**Table 1**
Atomic ratios and modulator concentration as determined by XPS. Two spots on each sample were measured and analyzed. The modulator concentration is approximated based on the integration of the wide scan.

| COF | Atomic ratios | | | | | Modulator concentration |
|---|---|---|---|---|---|---|
| | C1s | N1s | O1s | F1s | Cl2p | [mol %] |
| F-modulated $Me_3$TFB-BD | 88.8 | 9.5 | 1.0 | 0.7 | – | 21 ± 9 |
| Cl-modulated $Me_3$TFB-BD | 90.8 | 8.3 | – | – | 0.9 | 24 ± 2 |

To study the stability in water, all modulated COFs and $Me_3$TFB-OMeBD were immersed for five days into deionized water and upon re-isolation and drying at 120 °C overnight, the PXRD patterns were recorded again. All COFs could be isolated from the vials used for the water stability test, which allowed re-analysis by PXRD, showing that none of the harvested materials were completely amorphized. Except from Cl-modulated COF and $Me_3$TFB-OMeBD, all other COFs were found to be stable under the tested conditions, as indicated by the retained PXRD patterns (SI Fig. 16).

To investigate the morphology of the COFs, Scanning Electron Microscopy (SEM) was carried out (SI Figures S31-38). The samples do not have spherical particles with a certain particle size distribution, but the COF powder consists of aggregates of different sizes. $Me_3$TFB-BD and all modulated COFs consist of worm-like cylinders grown together in an irregular fashion. The diameter of the cylinders is in the range of a few hundred nanometers while their length is in the micrometer regime. In the case of OMe-modulated COF, the porous surface of those cylinders was observed (SI Fig. 32). $Me_3$TFB-OMeBD shows a fluffy morphology as also observed for other benzidine-based COFs [59].

### 3.2. Gas adsorption studies

In order to determine whether the modulated COFs are promising candidates for gas separation applications, nitrogen and carbon dioxide sorption measurements have been conducted at 273 K and 295 K (SI Figs. 39–45). While the $CF_3$-modulated COF was a good example to demonstrate the characterization, the gas adsorption and IAST selectivity is exemplary discussed based on the OMe-modulated COF. We have chosen the OMe-COF because the directly synthesized $Me_3$TFB-OMeBD was the only COF that we could obtain for a comparison between the direct, *i.e.* modulator-free, condensation and the modulator approach. The adsorption isotherms at 273 K and 295 K of nitrogen and carbon dioxide of OMe-modulated COF are linear (Fig. 4A). The maximum quantity adsorbed of nitrogen at 273 K was 0.14 mmol/g at 1.33 bar and for carbon dioxide 0.84 mmol/g at 1.05 bar. The quantities adsorbed of $N_2$ and $CO_2$ for the other modulated COFs can be found in SI Table 5. At 273 K, many adsorption isotherms were not well resolved in the low pressure range due to the low adsorption quantities, which were most probably not well resolved anymore due to the accuracy of the pressure transducer. This inaccuracy became even more pronounced in the adsorption isotherms at 295 K. The same OMe-modulated COF adsorbed 0.08 mmol/g of nitrogen and 0.64 mmol/g of carbon dioxide at 1.33 bar and 295 K. These values are significantly lower than those reported for various related systems. For example, for porous imine-based networks the amounts of adsorbed $CO_2$ are reported to be ~1.8–3.3 mmol/g at 273 K, and ~1–2.4 mmol/g at 298 K [31,60]. Benzimidazole COFs are reported to have 2.68–3.45 mmol/g $CO_2$ adsorption at 273 K and 1.82–2.32 mmol/g at 298 K [61]. A carboxylic acid-functionalized imine-linked COF even showed carbon dioxide adsorptions of 3.95 and 1.73 mmol/g at 273 K and 298 K, respectively [26]. These differences can be rationalized by the relative low number of polarizable groups in our modulated COFs compared to those reported in literature.

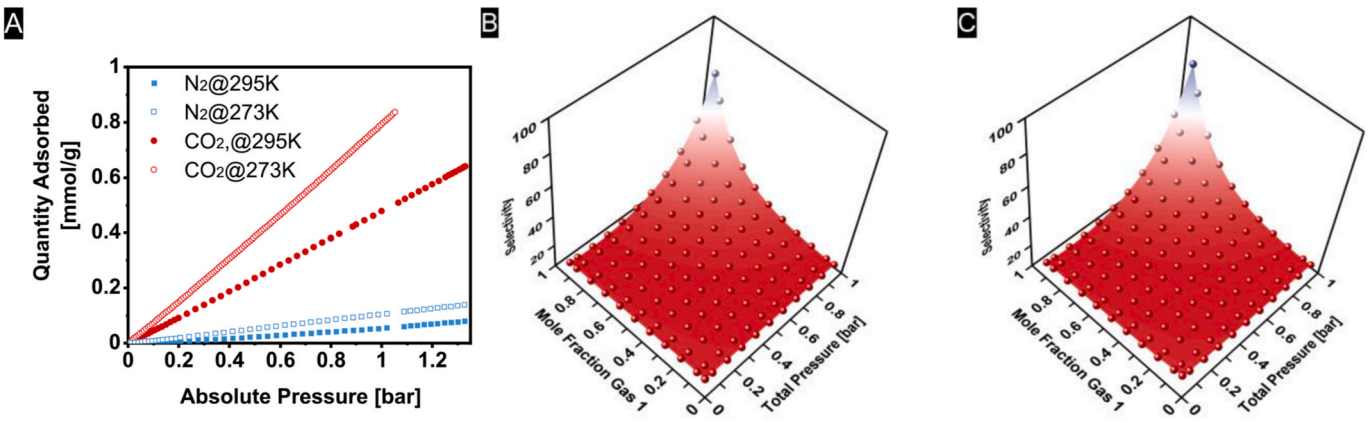


**Fig. 4.** (A) Nitrogen and carbon dioxide adsorption isotherms at 273 K and 295 K, (B) $CO_2/N_2$ IAST selectivity of $CF_3$-modulated COF at 273 K, and (C) $CO_2/N_2$ IAST selectivity of $CF_3$-modulated COF at 295 K.

These isotherms were then used to calculate the IAST selectivity with our recently developed GraphIAST [52]over pressures from 0.1 to 1.0 bar and mole fractions ranging from 0.05 to 0.95. The obtained three-dimensional IAST selectivity plots at 273 K and 295 K are shown in Fig. 4B and C. At lower mole fractions or pressures, the selectivity drops below 10. Overall the IAST selectivity is lower compared to existing literature that reports selectivity values between 31 and 100 for imine networks [31,60] and benzimidazole [61], azine [27] or imine [26] COFs, and Mahato et al. studied a Covalent Triazine Framework (CTF) with a $CO_2/N_2$ selectivity as high as 185.8 at a mole fraction of 0.15 carbon dioxide and 1 bar and 273 K [30].

The low quantities adsorbed and the low selectivity values of our modulated COFs are not high enough to compensate for the energy and resources needed to synthesize them. Therefore, the modulated COFs are not suitable for gas separation applications. From Fig. 4B and C, it also becomes apparent that the $CO_2/N_2$ IAST selectivity significantly increases at higher pressures and higher $CO_2$ mole fractions. Despite the good selectivity values of 37 ± 23 (mole fraction 0.8 at 1 bar) to 70 ± 50 (mole fraction 0.95 at 1 bar) at 273 K and 40 ± 33 (mole fraction 0.8 at 1 bar) to 75 ± 71 (mole fraction 0.95 at 1 bar) at 295 K, the error margins are currently still very high. Furthermore, to the best of our knowledge, all carbon capture applications require good selectivities at lower mole fractions.

In industrial processes, the concentration of carbon dioxide is

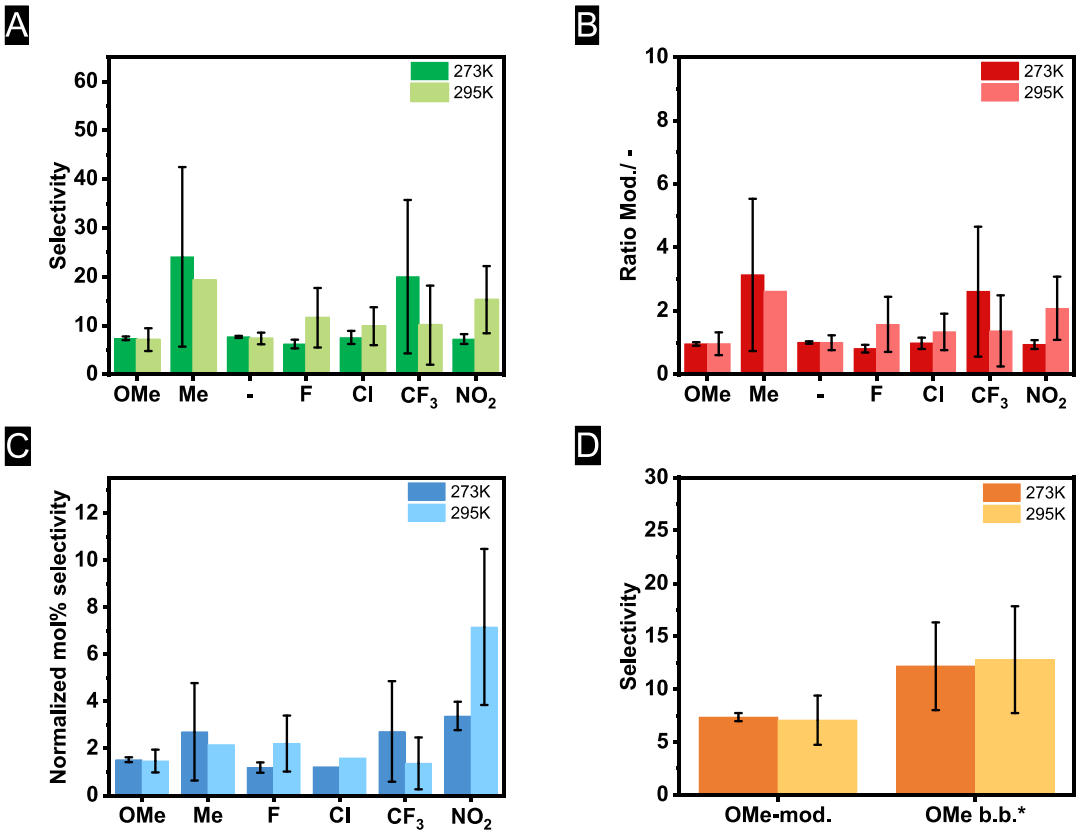


**Fig. 5.** $CO_2/N_2$ IAST selectivity of (A) modulated COFs, (B) normalized to unmodulated $Me_3$TFB-BD, (C) normalized to the incorporated modulator concentration, and (D) comparison of $CO_2/N_2$ IAST selectivity OMe-modulated COF vs. $Me_3$TFB-OMeBD. * Mod. stands for modulator (referred to as OMe-modulator) and b.b. stands for building block, here *o*-dianisidine.

significantly higher compared to the atmosphere. Flue gas, for example, contains between 10 and 25 vol% carbon dioxide [62]. Capturing the carbon dioxide and separate it from the other gases before the flue gas gets diluted by the atmosphere would be more efficient. Within this context a mole fraction 0.15 at 1 bar was chosen to study the performance of our modulated COFs (Fig. 5). The corresponding $CO_2/N_2$ IAST selectivity values range from 6 to 24 at 273 K and 7 to 20 at 295 K (Fig. 5A). Also the highest value is below selectivity values of channel-wall functionalized COFs already reported in imine-linked literature [26,31,60], and comparable to imine COFs with only backbone functionalization [63,64]. However, the higher IAST selectivity values for $CF_3$- and Me-modulated COF indicate at first a preferred adsorption of carbon dioxide in these two functional COFs. However, triplicate analysis revealed that the error margins for these selectivity calculations and their underlying isotherms are too large to draw this conclusion. Especially for Me-modulated COFs, it was difficult to record nitrogen isotherms. At 295 K, we were only able to measure an isotherm for one of the three Me-modulated COFs.

The different functional groups on the modulators range from electron-donating to electron-withdrawing groups, which could influence the $CO_2/N_2$ selectivity. To further analyze any relation between the type of functional group and the $CO_2/N_2$ selectivity, the $CO_2/N_2$ IAST selectivity was plotted against the Hammett parameters of the group under investigation (SI Fig. 46). However, no correlation between the Hammett parameter and the $CO_2/N_2$ IAST selectivity was found. We hypothesize that the low fraction of modulator within the samples is not enough to reveal the influence of electron donating and electron withdrawing groups on the $CO_2/N_2$ IAST selectivity.

To further analyze the data and normalize the IAST selectivity of all modulated COFs, the IAST selectivity of – the modulator-free – $Me_3$TFB-BD was also determined at 1.0 bar and a mole fraction of 0.15 (Fig. 5B). This enabled us to investigate whether the modulators have an advantageous effect compared to COFs without functional groups on the resulting IAST selectivity. Based on this normalization, the higher ratios for $CF_3$- and Me-modulated COFs are again not significant since the error margins are too large and the other modulated COFs have ratios of ~1, indicating that they have a similar IAST selectivity than the one of $Me_3$TFB-BD.

Next, the relation between the IAST selectivity and the concentration of modulator within the framework was studied. Since each modulator is incorporated in different amounts, these amounts need to be taken into account. Therefore, we normalized the spectrum by the average of the modulator concentration (Fig. 5C). As the functional groups of the modulators vary from electron-donating to electron-withdrawing, the normalized IAST selectivity was compared in line with the Hammett parameter. The results do not show a trend based on the electronic properties of the modulators and no functional group was outstanding. The interpretation of the data was mainly hampered again by the large error margins, which are related to the accuracy of the pressure transducer. Additionally, we hypothesize that these low amounts of adsorbed gases and the low IAST selectivity values are related to the concentration of modulator within the COF.

Thus, we synthesized and analyzed $Me_3$TFB-OMeBD in triplicate to see whether the small amounts of functional groups in modulated COFs are simply not enough for a clear $CO_2/N_2$ IAST selectivity. By comparing the IAST selectivity of OMe-modulated COF to $Me_3$TFB-OMeBD, it can be seen that the IAST selectivity almost doubles when more functional groups are present in the framework (Fig. 5D). Therefore, more functional groups seem to be advantageous for higher selective COF behavior. As not all functional building blocks are always compatible with the formation of a crystalline COF, it is of importance to develop synthetic routes for such structural variation, which will enable controlled analysis of the structure-property relationships of COFs in gas separation.

## 4. Conclusions

In conclusion, we have incorporated a series of functionalized modulators in $Me_3$TFB-BD COF frameworks and studied their performance in $CO_2/N_2$ gas separation, also in comparison to the pristine $Me_3$TFB-BD COF. Next to the imine linkage, which can already provide interactions with carbon dioxide, additional functional groups in the framework can tailor the COF towards improved COF-gas interactions. We have employed modulators, which are known to improve COF porosity, and additional functional groups in the *para* position (OMe, Me, F, Cl, $CF_3$, $NO_2$) were thought to enhance COF-$CO_2$ interactions. The higher reactivity of benzidine, compared to that of all modulators, leads to relatively lower modulator embedding than the 30 mol% of modulator present in the reaction mixtures, ranging from 2.1 mol% for the $NO_2$-modulated COF to 8.9 mol% for the Me-modulated COF. All BET surface areas remain high (>1800 $m^2/g$) and prove the high porosity of the modulated COFs.

These modulated COFs showed moderate quantities of adsorbed carbon dioxide in gas separation experiments, while the $CO_2/N_2$ IAST selectivity values are comparable ($S = 6–24$ for the different modulators at 273 K) to imine-COFs without channel-wall functionalization under flue gas conditions. The low number of functional, polarizable groups within the COF hampered displaying any trends of favorable $CO_2$ interactions with a certain functional group, but for all it was found that an increase in functional group embedding leads to higher $CO_2/N_2$ IAST selectivity values.

## Funding sources

This study was supported by the Dutch Research Council (NWO, START-UP Grant 740.018.004, to LdS).

## CRediT authorship contribution statement

**Ellen Dautzenberg:** Writing – original draft, Visualization, Project administration, Investigation, Formal analysis, Conceptualization. **Frank W. Claassen:** Investigation. **Louis C.P.M. de Smet:** Writing – original draft, Visualization, Supervision, Project administration, Funding acquisition.

## Declaration of competing interest

The authors declare that they have no known competing financial interests or personal relationships that could have appeared to influence the work reported in this paper.

## Data availability

Data will be made available on request.

## Acknowledgment

This work was supported by the Dutch Research Council (NWO, START-UP Grant 740.018.004, to LdS). The authors thank Prof. Han Zuilhof (WUR) and Prof. Rahul Banerjee (IISER Kolkata) for fruitful discussions and Barend van Lagen and Julian Engelhardt (both WUR) for technical assistance.

## Appendix A. Supplementary data

Supplementary data to this article can be found online at https://doi.org/10.1016/j.micromeso.2022.112318.

## References


[1] M. Thommes, K. Kaneko, A.V. Neimark, J.P. Olivier, F. Rodriguez-Reinoso, J. Rouquerol, K.S.W. Sing, Physisorption of gases, with special reference to the evaluation of surface area and pore size distribution (IUPAC Technical Report), Pure Appl. Chem. 87 (2015) 1051–1069, https://doi.org/10.1515/pac-2014-1117.

[2] A.P. Côté, A.I. Benin, N.W. Ockwig, M. O'Keeffe, A.J. Matzger, O.M. Yaghi, Porous, crystalline, covalent organic frameworks, Science (80-.) 310 (2005) 1166–1170, https://doi.org/10.1126/science.1120411.

[3] J.L. Segura, M.J. Mancheño, F. Zamora, Covalent organic frameworks based on Schiff-base chemistry: synthesis, properties and potential applications, Chem. Soc. Rev. 45 (2016) 5635–5671, https://doi.org/10.1039/c5cs00878f.

[4] S. Kandambeth, K. Dey, R. Banerjee, Covalent organic frameworks: chemistry beyond the structure, J. Am. Chem. Soc. 141 (2019) 1807–1822, https://doi.org/10.1021/jacs.8b10334.

[5] C.R. Deblase, K.E. Silberstein, T.T. Truong, H.D. Abruña, W.R. Dichtel, B-ketoenamine-linked covalent organic frameworks capable of pseudocapacitive energy storage, J. Am. Chem. Soc. 135 (2013) 16821–16824, https://doi.org/10.1021/ja409421d.

[6] L. Ascherl, E.W. Evans, M. Hennemann, D. Di Nuzzo, A.G. Hufnagel, M. Beetz, R. H. Friend, T. Clark, T. Bein, F. Auras, Solvatochromic covalent organic frameworks, Nat. Commun. 9 (2018) 3802, https://doi.org/10.1038/s41467-018-06161-w.

[7] H. Wang, H. Wang, Z. Wang, L. Tang, G. Zeng, P. Xu, M. Chen, T. Xiong, C. Zhou, X. Li, D. Huang, Y. Zhu, Z. Wang, J. Tang, Covalent organic framework photocatalysts: structures and applications, Chem. Soc. Rev. 49 (2020) 4135–4165, https://doi.org/10.1039/d0cs00278j.

[8] N. Singh, D. Yadav, S.V. Mulay, J.Y. Kim, N.J. Park, J.O. Baeg, Band gap engineering in Solvochromic 2D covalent organic framework photocatalysts for visible light-driven enhanced solar fuel production from carbon dioxide, ACS Appl. Mater. Interfaces 13 (2021) 14122–14131, https://doi.org/10.1021/acsami.0c21117.

[9] H. Fan, M. Peng, I. Strauss, A. mundstock, H. Meng, J. Caro, High-flux vertically aligned 2D covalent organic framework membrane with enhanced hydrogen separation, J. Am. Chem. Soc. 142 (2020) 2–7, https://doi.org/10.1021/jacs.0c00927.

[10] S.J. Rowan, S.J. Cantrill, G.R.L. Cousins, J.K.M. Sanders, J.F. Stoddart, Dynamic covalent chemistry, Angew. Chem. Int. Ed. 41 (2002) 898–952, https://doi.org/10.1002/1521-3773(20020315)41:6<898::aid-anie898>3.0.co;2-e.

[11] J. Hu, S.K. Gupta, J. Ozdemir, M.H. Beyzavi, Applications of dynamic covalent chemistry concept toward tailored covalent organic framework nanomaterials: a review, ACS Appl. Nano Mater. 3 (2020) 6239–6269, https://doi.org/10.1021/acsanm.0c01327.

[12] B.J. Smith, L.R. Parent, A.C. Overholts, P.A. Beaucage, R.P. Bisbey, A.D. Chavez, N. Hwang, C. Park, A.M. Evans, N.C. Gianneschi, W.R. Dichtel, Colloidal covalent organic frameworks, ACS Cent. Sci. 3 (2017) 58–65, https://doi.org/10.1021/acscentsci.6b00331.

[13] E. Vitaku, W.R. Dichtel, Synthesis of 2D imine-linked covalent organic frameworks through formal transimination reactions, J. Am. Chem. Soc. 139 (2017) 12911–12914, https://doi.org/10.1021/jacs.7b06913.

[14] H. Schiff, Mittheilungen aus dem Universitätslaboratorium in Pisa: eine neue Reihe organischer Basen, Justus Liebigs Ann. Chem. 131 (1864) 118–119, https://doi.org/10.1002/JLAC.18641310113.

[15] O. Talu, Needs, status, techniques and problems with binary gas adsorption experiments, Adv. Colloid Interface Sci. 76–77 (1998) 227–269, https://doi.org/10.1016/S0001-8686(98)00048-7.

[16] A.L. Myers, J.M. Prausnitz, Thermodynamics of mixed-gas adsorption, AIChE J. 11 (1965) 121–127, https://doi.org/10.1002/AIC.690110125.

[17] P. Wang, Y. Peng, C. Zhu, R. Yao, H. Song, L. Kun, W. Yang, P. Wang, Y. Peng, C. Zhu, R. Yao, H. Song, L. Kun, W. Yang, Single-phase covalent organic framework staggered stacking nanosheet membrane for CO2-selective separation, Angew. Chem. Int. Ed. 60 (2021) 19047–19052, https://doi.org/10.1002/ANIE.202106346.

[18] N.F. Cessford, N.A. Seaton, T. Düren, Evaluation of ideal adsorbed solution theory as a tool for the design of metal-organic framework materials, Ind. Eng. Chem. Res. 51 (2012) 4911–4921, https://doi.org/10.1021/ie202219w.

[19] X. An, K. Zhao, W. Zhang, J. Yang, Y. Liao, L. Wang, D. Fu, Tailoring the pore structure modified with functional groups for superior CO2 adsorption capacity and the selectivity of separation, Fuel 309 (2022), 122175, https://doi.org/10.1016/J.FUEL.2021.122175.

[20] X. Cai, F. Gharagheizi, L.W. Bingel, D. Shade, K.S. Walton, D.S. Sholl, A collection of more than 900 gas mixture adsorption experiments in porous materials from literature meta-analysis, Ind. Eng. Chem. Res. 60 (2021) 639–651, https://doi.org/10.1021/acs.iecr.0c05398.

[21] F. Gharagheizi, D.S. Sholl, Comprehensive assessment of the accuracy of the ideal adsorbed solution theory for predicting binary adsorption of gas mixtures in porous materials, Ind. Eng. Chem. Res. 61 (2022) 727–739, https://doi.org/10.1021/acs.iecr.1c03876.

[22] S.P. Lee, N. Mellon, A.M. Shariff, J.M. Leveque, Geometry variation in porous covalent triazine polymer (CTP) for CO2 adsorption, New J. Chem. 42 (2018) 15488–15496, https://doi.org/10.1039/C8NJ00638E.

[23] S.P. Lee, N. Mellon, A.M. Shariff, J.M. Leveque, High-pressure CO2-CH4 selective adsorption on covalent organic polymer, J. Nat. Gas Sci. Eng. 50 (2018) 139–146, https://doi.org/10.1016/J.JNGSE.2017.11.024.

[24] B. Liu, L. Yu, H. Wang, X. Ma, Z. Zeng, L. Li, Experimental and molecular perspective on VOCs adsorption and separation: study of the surface heterogeneity and oxygen functionalizing, Chem. Eng. J. 435 (2022), 135069, https://doi.org/10.1016/J.CEJ.2022.135069.

[25] A. Kundu, K. Sillar, J. Sauer, Predicting adsorption selectivities from pure gas isotherms for gas mixtures in metal–organic frameworks, Chem. Sci. 11 (2020) 643–655, https://doi.org/10.1039/C9SC03008E.

[26] N. Huang, X. Chen, R. Krishna, D. Jiang, Two-dimensional covalent organic frameworks for carbon dioxide capture through channel-wall functionalization, Angew. Chem. Int. Ed. 54 (2015) 2986–2990, https://doi.org/10.1002/anie.201411262.

[27] L. Stegbauer, M.W. Hahn, A. Jentys, G. Savasci, C. Ochsenfeld, J.A. Lercher, B. V. Lotsch, Tunable water and CO2 sorption properties in isostructural azine-based covalent organic frameworks through polarity engineering, Chem. Mater. 27 (2015) 7874–7881, https://doi.org/10.1021/acs.chemmater.5b02151.

[28] J. Lan, D. Cao, W. Wang, B. Smit, Doping of alkali, alkaline-earth, and transition metals in covalent-organic frameworks for enhancing CO2 capture by first-principles calculations and molecular simulations, ACS Nano 4 (2010) 4225–4237, https://doi.org/10.1021/nn100962r.

[29] R. Gomes, A. Bhaumik, A new triazine functionalized luminescent covalent organic framework for nitroaromatic sensing and CO2 storage, RSC Adv. 6 (2016) 28047–28054, https://doi.org/10.1039/C6RA01717G.

[30] M. Mahato, S. Nam, R. Tabassian, S. Oh, V.H. Nguyen, I.K. Oh, Electronically conjugated multifunctional covalent triazine framework for unprecedented CO2 selectivity and high-power flexible supercapacitor, Adv. Funct. Mater. 32 (2022), 2107442, https://doi.org/10.1002/ADFM.202107442.

[31] S.K. Das, X. Wang, M.M. Ostwal, Z. Lai, A highly stable microporous covalent imine network adsorbent for natural gas upgrading and flue gas CO2 capture, Separ. Purif. Technol. 170 (2016) 68–77, https://doi.org/10.1016/J.SEPPUR.2016.06.016.

[32] Y. Wang, C. Kang, Z. Zhang, A.K. Usadi, D.C. Calabro, L.S. Baugh, Y. Di Yuan, D. Zhao, Evaluation of schiff-base covalent organic frameworks for CO2 capture: structure-performance relationships, stability, and performance under wet conditions, ACS Sustain. Chem. Eng. 10 (2022) 332–341, https://doi.org/10.1021/acssuschemeng.1c06318.

[33] G.Y. Lee, J. Lee, H.T. Vo, S. Kim, H. Lee, T. Park, Amine-functionalized covalent organic framework for efficient SO2 Capture with high reversibility, Sci. Rep. 7 (2017) 1–10, https://doi.org/10.1038/s41598-017-00738-z.

[34] X. Chen, L. Xia, R. Pan, X. Liu, Covalent organic framework mesocrystals through dynamic modulator manipulated mesoscale self-assembly of imine macrocycle precursors, J. Colloid Interface Sci. 568 (2020) 76–80, https://doi.org/10.1016/J.JCIS.2020.02.046.

[35] I. Castano, A.M. Evans, H. Li, E. Vitaku, M.J. Strauss, J.-L. Brédas, N.C. Gianneschi, W.R. Dichtel, Chemical control over nucleation and anisotropic growth of two-dimensional covalent organic frameworks, ACS Cent. Sci. 5 (2019) 1892–1899, https://doi.org/10.1021/ACSCENTSCI.9B00944.

[36] W. Liu, X. Li, C. Wang, H. Pan, W. Liu, K. Wang, Q. Zeng, R. Wang, J. Jiang, A scalable general synthetic approach toward ultrathin imine-linked two-dimensional covalent organic framework nanosheets for photocatalytic CO2 reduction, J. Am. Chem. Soc. 141 (2019) 17431–17440, https://doi.org/10.1021/JACS.9B09502.

[37] S. Wang, Z. Zhang, H. Zhang, A.G. Rajan, N. Xu, Y. Yang, Y. Zeng, P. Liu, X. Zhang, Q. Mao, Y. He, J. Zhao, B.G. Li, M.S. Strano, W.J. Wang, Reversible polycondensation-termination growth of covalent-organic-framework spheres, fibers, and films, Matter 1 (2019) 1592–1605, https://doi.org/10.1016/J.MATT.2019.08.019.

[38] M. Calik, T. Sick, M. Dogru, M. Döblinger, S. Datz, H. Budde, A. Hartschuh, F. Auras, T. Bein, From highly crystalline to outer surface-functionalized covalent organic frameworks-A modulation approach, J. Am. Chem. Soc. 138 (2016) 1234–1239, https://doi.org/10.1021/jacs.5b10708.

[39] D. Zhu, L.B. Alemany, W. Guo, R. Verduzco, Enhancement of crystallinity of imine-linked covalent organic frameworks via aldehyde modulators, Polym. Chem. 11 (2020) 4464–4468, https://doi.org/10.1039/D0PY00776E.

[40] R.A. Maia, F.L. Oliveira, M. Nazarkovsky, P.M. Esteves, Crystal engineering of covalent organic frameworks based on hydrazine and hydroxy-1,3,5-triformylbenzenes, Cryst. Growth Des. 18 (2018) 5682–5689, https://doi.org/10.1021/ACS.CGD.8B01110.

[41] T. Ma, E.A. Kapustin, S.X. Yin, L. Liang, Z. Zhou, J. Niu, L.-H. Li, Y. Wang, J. Su, J. Li, X. Wang, W.D. Wang, W. Wang, J. Sun, O.M. Yaghi, Single-crystal x-ray diffraction structures of covalent organic frameworks, Science (80-.) 361 (2018) 48–52, https://doi.org/10.1126/SCIENCE.AAT7679.

[42] L. Liang, Y. Qiu, W.D. Wang, J. Han, Y. Luo, W. Yu, G.-L. Yin, Z.-P. Wang, L. Zhang, J. Ni, J. Niu, J. Sun, T. Ma, W. Wang, Non-interpenetrated single-crystal covalent organic frameworks, Angew. Chem. Int. Ed. 59 (2020) 17991–17995, https://doi.org/10.1002/ANIE.202007230.

[43] L.P. Hammett, Some relations between reaction rates and equilibrium constants, Chem. Rev. 17 (1935) 125–136, https://doi.org/10.1021/cr60056a010.

[44] L.P. Hammett, The effect of structure upon the reactions of organic compounds. Benzene derivatives, J. Am. Chem. Soc. 59 (1937) 96–103, https://doi.org/10.1021/ja01280a022.

[45] C. Hansch, A. Leo, S.H. Unger, K.H. Kim, D. Nikaitani, E.J. Lien, "Aromatic" substituent constants for structure-activity correlations†, J. Med. Chem. 16 (1973) 1207–1216, https://doi.org/10.1021/jm00269a003.

[46] C. Hansch, A. Leo, R.W. Taft, A survey of Hammett substituent constants and resonance and field parameters, Chem. Rev. 91 (1991) 165–195, https://doi.org/10.1021/cr00002a004.

[47] S.L. Keenan, K.P. Peterson, K. Peterson, K. Jacobson, Determination of Hammett equation rho constant for the hydrolysis of p-nitrophenyl benzoate esters, J. Chem. Educ. 85 (2008) 558–560, https://doi.org/10.1021/ed085p558.
[48] D. Schultz, J.R. Nitschke, Designing multistep transformations using the Hammett equation: imine exchange on a Copper(I) template, J. Am. Chem. Soc. 128 (2006) 9887–9892, https://doi.org/10.1021/ja061841u.
[49] S.K. Schoustra, J.A. Dijksman, H. Zuilhof, M.M.J. Smulders, Molecular control over vitrimer-like mechanics – tuneable dynamic motifs based on the Hammett equation in polyimine materials, Chem. Sci. 12 (2021) 293–302, https://doi.org/10.1039/D0SC05458E.
[50] E. Dautzenberg, M. Lam, G. Li, L.C.P.M. de Smet, Enhanced surface area and reduced pore collapse of methylated, imine-linked covalent organic frameworks, Nanoscale 13 (2021) 19446–19452, https://doi.org/10.1039/d1nr05911d.
[51] K.S. Walton, D.S. Sholl, Predicting multicomponent adsorption: 50 years of the ideal adsorbed solution theory, AIChE J. 61 (2015) 2757–2762, https://doi.org/10.1002/AIC.14878.
[52] E. Dautzenberg, S. van Hurne, M.M.J. Smulders, L.C.P.M. de Smet, GraphIAST: a graphical user interface software for Ideal Adsorption Solution Theory (IAST) calculations, Comput. Phys. Commun. (2022), 108494, https://doi.org/10.1016/J.CPC.2022.108494.
[53] B.J. Smith, A.C. Overholts, N. Hwang, W.R. Dichtel, Insight into the crystallization of amorphous imine-linked polymer networks to 2D covalent organic frameworks, Chem. Commun. 52 (2016) 3690–3693, https://doi.org/10.1039/c5cc10221a.
[54] M. Hesse, H. Meier, B. Zeeh, Spectroscopic Methods in Organic Chemistry, second ed., Georg Thieme Verlag, 2008.
[55] E. Dautzenberg, M. Lam, T. Nikolaeva, W.M.J. Franssen, B. van Lagen, I.P.A. M. Gerrits-Benneheij, N. Kosinov, G. Li, L.C.P.M. de Smet, Insight into the crystallization of amorphous imine-linked polymer networks to 2D covalent organic frameworks, J. Phys. Chem. C 126 (2022) 21338–21347, https://doi.org/10.1021/acs.jpcc.2c04586.
[56] G.M.F. Rouquerol, J. Rouquerol, K.S.W. Sing, P. Llewllyn, Adsorption by Powders and Porous Solids, second ed., Academic Press, Oxford, U.K., 2014.
[57] D.R. Baer, K. Artyushkova, C.R. Brundle, J.E. Castle, M.H. Engelhard, K.J. Gaskell, J.T. Grant, R.T. Haasch, M.R. Linford, C.J. Powell, A.G. Shard, P.M.A. Sherwood, V. S. Smentkowski, Practical guides for x-ray photoelectron spectroscopy: first steps in planning, conducting, and reporting XPS measurements, J. Vac. Sci. Technol. A Vacuum, Surfaces, Film. 37 (2019), 031401, https://doi.org/10.1116/1.5065501.
[58] C.D. Easton, C. Kinnear, S.L. McArthur, T.R. Gengenbach, Practical guides for x-ray photoelectron spectroscopy: analysis of polymers, J. Vac. Sci. Technol. A Vacuum, Surfaces, Film. 38 (2020), 023207, https://doi.org/10.1116/1.5140587.
[59] Y. Liu, A. Dikhtiarenko, N. Xu, J. Sun, J. Tang, K. Wang, B. Xu, Q. Tong, H. J. Heeres, S. He, J. Gascon, Y. Fan, Triphenylphosphine-based covalent organic frameworks and heterogeneous Rh-P-COFs catalysts, Chem. Eur J. 26 (2020) 12134–12139, https://doi.org/10.1002/CHEM.202002150.
[60] N. Popp, T. Homburg, N. Stock, J. Senker, Porous imine-based networks with protonated imine linkages for carbon dioxide separation from mixtures with nitrogen and methane, J. Mater. Chem. A. 3 (2015) 18492–18504, https://doi.org/10.1039/C5TA02504D.
[61] S. Altarawneh, T. Islamoğlu, A.K. Sekizkardes, H.M. El-Kaderi, Effect of acid-catalyzed formation rates of benzimidazole-linked polymers on porosity and selective CO2 capture from gas mixtures, Environ. Sci. Technol. 49 (2015) 4715–4723, https://doi.org/10.1021/es505760w.
[62] I.A. Principe, A.J. Fletcher, Adsorption selectivity of CO2 over CH4, N2 and H2 in melamine–resorcinol–formaldehyde xerogels, Adsorption 26 (2020) 723–735, https://doi.org/10.1007/S10450-020-00203-W/FIGURES/10.
[63] Y. Zu, J. Li, X. Li, T. Zhao, H. Ren, F. Sun, Imine-linked porous aromatic frameworks based on spirobifluorene building blocks for CO2 separation, Microporous Mesoporous Mater. 334 (2022), 111779, https://doi.org/10.1016/J.MICROMESO.2022.111779.
[64] S. Zhao, B. Dong, R. Ge, C. Wang, X. Song, W. Ma, Y. Wang, C. Hao, X. Guo, Y. Gao, Channel-wall functionalization in covalent organic frameworks for the enhancement of CO2 uptake and CO2/N2 selectivity, RSC Adv. 6 (2016) 38774–38781, https://doi.org/10.1039/C6RA04859E.